AGU PUBLICATIONS

Geophysical Research Letters

RESEARCH LETTER
10.1002/2014GL059651

**Key Points:**
- The dry deposition scheme (Wesely, 1989) is corrected and optimized in CESM
- Dry deposition velocity and surface $O_3$ simulations are significantly improved
- Linking deposition to LAI is key to simulate $O_3$ responses to vegetation changes

**Supporting Information:**
- Readme
- Figure S1
- Figure S2

**Correspondence to:**
M. Val Martin,
mval@atmos.colostate.edu

**Citation:**
Val Martin, M., C. L. Heald, and S. R. Arnold (2014), Coupling dry deposition to vegetation phenology in the Community Earth System Model: Implications for the simulation of surface $O_3$, *Geophys. Res. Lett.*, *41*, doi:10.1002/2014GL059651.

Received 19 FEB 2014
Accepted 1 APR 2014
Accepted article online 2 APR 2014

# Coupling dry deposition to vegetation phenology in the Community Earth System Model: Implications for the simulation of surface $O_3$

**M. Val Martin[1], C. L. Heald[2], and S. R. Arnold[3]**

[1]Atmospheric Science Department, Colorado State University, Fort Collins, Colorado, USA, [2]Department of Civil and Environmental Engineering, Massachusetts Institute of Technology, Cambridge, Massachusetts, USA, [3]Institute for Climate and Atmospheric Science, School of Earth and Environment, University of Leeds, Leeds, UK

**Abstract** Dry deposition is an important removal process controlling surface ozone. We examine the representation of this ozone loss mechanism in the Community Earth System Model. We first correct the dry deposition parameterization by coupling the leaf and stomatal vegetation resistances to the leaf area index, an omission which has adversely impacted over a decade of ozone simulations using both the Model for Ozone and Related chemical Tracers (MOZART) and Community Atmospheric Model-Chem (CAM-Chem) global models. We show that this correction increases $O_3$ dry deposition velocities over vegetated regions and improves the simulated seasonality in this loss process. This enhanced removal reduces the previously reported bias in summertime surface $O_3$ simulated over eastern U.S. and Europe. We further optimize the parameterization by scaling down the stomatal resistance used in the Community Land Model to observed values. This in turn further improves the simulation of dry deposition velocity of $O_3$, particularly over broadleaf forested regions. The summertime surface $O_3$ bias is reduced from 30 ppb to 14 ppb over eastern U.S. and 13 ppb to 5 ppb over Europe from the standard to the optimized scheme, respectively. $O_3$ deposition processes must therefore be accurately coupled to vegetation phenology within 3-D atmospheric models, as a first step toward improving surface $O_3$ and simulating $O_3$ responses to future and past vegetation changes.

## 1. Introduction

Surface ozone ($O_3$) is a harmful air pollutant that is toxic to humans and ecosystems. $O_3$ concentrations in the troposphere are controlled by a balance among chemical production, stratospheric influx, and loss processes. A major loss process for $O_3$ is surface dry deposition, accounting for about 20% of the $O_3$ lost in the troposphere [*Wild*, 2007]. The majority of this $O_3$ removal occurs over vegetation, mainly by direct uptake through the stomatal pores of plants and by direct deposition over the leaf cuticles [e.g., *Wesely*, 1989].

Changes in vegetation as a result of human activities and climate change are of great concern for $O_3$ air quality [e.g., *Sanderson et al.*, 2003; *Ganzeveld et al.*, 2010; *Wu et al.*, 2012]. For example, deforestation may decrease foliar uptake, prompting a rise in $O_3$ concentration. In addition, changes in vegetation affect emissions of $O_3$ precursors (e.g., biogenic volatile organic compounds and soil $NO_x$ emissions), which in turn affect OH, an important oxidizing agent in the atmosphere that regulates the lifetime of the greenhouse gas methane.

Surface $O_3$ is challenging to simulate in 3-D atmospheric models [e.g., *Murazaki and Hess*, 2006; *Wu et al.*, 2007; *Lamarque et al.*, 2012], due to the nonlinearity of the chemistry, the complexity of physical process, and the heterogeneity of precursor emissions. A recent well-known issue in some models is the positive bias of surface ozone of more than 10 ppb over eastern U.S. and Europe during the summer [e.g., *Murazaki and Hess*, 2006; *Fiore et al.*, 2009; *Reidmiller et al.*, 2009; *Lamarque et al.*, 2012]. For example, *Murazaki and Hess* [2006] reported a very large positive bias (40–60 ppb) for the maximum daily 8 h averaged (MDA8) $O_3$ over eastern U.S. in the summer with the Model for Ozone and Related chemical Tracers version 2 (MOZART-2). *Lamarque et al.* [2012] reported a similar bias for the Community Earth System Model (CESM) over the eastern U.S. and a bias of 10–30 ppb over Europe. A positive bias of 10–20 ppb was reported for summertime MDA8 $O_3$ over eastern U.S. in the multimodel Hemispheric Transport of Air Pollution study [*Reidmiller et al.*, 2009]. Most recently, *Lapina et al.* [2014] reported a consistent bias of 15 ppb for summertime daily $O_3$ over the eastern U.S. from the mean of three models: GEOS-Chem, GFDL AM3, and STEM.

## 2. Methods and Results

With the goal of understanding the role of the dry deposition in the persistent positive bias of surface $O_3$ over eastern U.S. and Europe, and the ability of the global CESM to properly simulate $O_3$ responses to vegetation changes, we review, evaluate, and optimize the dry deposition parameterization scheme in CESM. For this work, we use CESM driven by Modern Era Retrospective-Analysis (MERRA) reanalyzed meteorological fields from the NASA Global Modeling and Assimilation Office, with a 1.9° × 2.5° horizontal resolution, and 56 vertical levels between the surface and 0.02 hPa (including 13 levels up to 800 hPa). We employ CESM version 1.1.1 for the year 2001 and specified sea surface and sea ice distributions, i.e., we only allow fast land and atmospheric responses to occur. To simulate land surface processes, we use the Community Land Model version 4 (CLM4) [*Oleson et al.*, 2010]; for the atmospheric model, we use the Community Atmospheric Model version 4 (CAM4) [*Neale et al.*, 2013] fully coupled with the interactive gas-aerosol scheme CAM-Chem [*Lamarque et al.*, 2012]. The chemical mechanism contains full tropospheric $O_3$–$NO_x$–CO–VOC and aerosol phase chemistry, based on MOZART-4 [*Emmons et al.*, 2010].

The dry deposition scheme in CESM is based on the multiple-resistance approach originally described by *Wesely* [1989], with some updates discussed in *Emmons et al.* [2010] and *Lamarque et al.* [2012]. The dry deposition velocity ($V_d$) is computed as follows:

$$V_d = \frac{1}{R_a + R_b + R_c},$$

where $R_a$ is the aerodynamic resistance, $R_b$ is the quasi-laminar sublayer resistance above canopy, and $R_c$ is the surface resistance. For $O_3$ and over vegetated regions, $V_d$ is mainly driven by $R_c$ during the day since the effects of $R_a$ and $R_b$, which are dependent on meteorological conditions, are typically small [*Zhang et al.*, 2002]. $R_c$ is then computed as follows:

$$\frac{1}{R_c} = \frac{1}{R_s + R_m} + \frac{1}{R_{lu}} + \frac{1}{R_{cl}} + \frac{1}{R_g},$$

where $R_s$ is the stomatal resistance, $R_m$ is the leaf mesophyll resistance ($R_m$=0 s/cm for $O_3$), $R_{lu}$ is the upper canopy or leaf cuticle resistance, $R_{cl}$ is the lower canopy resistance, and $R_g$ is the ground resistance. This surface resistance scheme is commonly applied in both regional and global models, although different approaches are used to calculate the resistance components. For example, $R_s$ schemes range from simple parameterizations as a function of solar radiation and/or time of day [e.g., *Wesely*, 1989], one- or two-big-leaf approaches [e.g., *Collatz et al.*, 1991; *Zhang et al.*, 2002], to a multilayer leaf resistance models [e.g., *Baldocchi et al.*, 1987]. Typically, dry deposition schemes are used with fixed vegetation parameters. However, the evolution of Earth System Models in recent years provides the capability to couple the atmospheric composition to evolving vegetation [e.g., *Sanderson et al.*, 2007]. Here we couple the simulation of dry deposition loss of atmospheric species to the vegetation phenology represented in the CLM. In the land model, all the individual resistances in $R_c$ are computed at the level of each plant functional type (PFT). Then, the deposition velocity in each grid box is computed as the weighted mean over all land cover types available at each grid box [*Lamarque et al.*, 2012] and transferred to CAM-Chem through a coupler. At the same time, CAM-Chem provides CLM with the meteorological fields needed to determine the resistance components dependent on atmospheric conditions (e.g., $R_a$ and $R_b$).

Our investigation of and modifications to the dry deposition scheme revealed a series of oversimplifications in the implementation of the parameterization in the standard code for CAM-Chem (and the MOZART model upon which it is based, including MOZART-2, MOZART-3, and MOZART-4); these are summarized in Table 1. In the original dry deposition scheme, $R_s$ is based on the simple scheme described by *Wesely* [1989], in which this resistance is mainly determined by a parameter prescribed for each season and PFT. Thus, $R_s$ is not integrated over the canopy depth and neglects the leaf area index (LAI) dependence to account for the seasonality and the geographical distribution of the vegetation [*Baldocchi et al.*, 1987; *Gao and Wesely*, 1995]. In this work, we replace the standard *Wesely* [1989] $R_s$ scheme by the Ball-Berry $R_s$ scheme described by *Collatz et al.* [1991] and implemented in a global model by *Sellers et al.* [1996]. The Ball-Berry scheme relates the $R_s$ directly to the net leaf photosynthesis. Both parameters are computed in CLM and are dependent on environmental and canopy factors [*Oleson et al.*, 2010]. We use the LAI to integrate $R_s$ over the canopy depth for sunlit and shaded leaves. Monthly LAI in CLM (run with offline phenology) is derived from

**Table 1.** Summary of Major Changes in the CESM Dry Deposition Velocity Scheme[a]

| Original Scheme | Corrected Scheme |
|---|---|
| *Stomatal Resistance* ($R_s$) | |
| $R_s = r_s \left\{1 + \frac{1}{[200(G+0.1)]^2}\right\} \left\{\frac{400}{T_s(40-T_s)}\right\} \frac{D_{H_2O}}{D_x}$ | $\frac{1}{r_s} = m\frac{A}{c_s}\frac{e_s}{e_i}P_{atm} + b$ |
| [*Wesely*, 1989] | [*Collatz et al.*, 1991; *Sellers et al.*, 1996] |
| | $R_s = \frac{f_{sun} \times r_s^{sun}}{LAI} + \frac{(1 - f_{sun}) \times r_s^{sha}}{LAI}$ |
| *Leaf Cuticular Resistance* ($R_{lu}$) | |
| $R_{lu} = \frac{r_{lu}}{10^{-5}H + f_o}$ | $R_{lu} = \frac{r_{lu}}{LAI \times (10^{-5}H + f_o)}$ |
| [*Wesely*, 1989] | [*Gao and Wesely*, 1995] |

[a]The minimum stomatal resistance is $r_s$, $G$ is solar radiation, $T_s$ is surface air temperature $D_{H_2O}$ and $D_x$ are the molecular diffusivities for water vapor and for a specific gas $x$, $m$ is the Ball-Berry slope of the conductance-photosynthesis relationship as a function of PFT, $A$ is leaf photosynthesis calculated separately for sunlit and shaded leaves to give $r_s^{sun}$ and $r_s^{sha}$, $b$ is the minimum stomatal conductance when A $\leq$0, $c_s$ is the $CO_2$ partial pressure at the leaf surface, $e_s$ is the vapor pressure at the leaf surface, $e_i$ is the saturation vapor pressure inside the leaf and $P_{atm}$ is the atmospheric pressure, $f_{sun}$ is sunlit fraction of canopy, LAI is the leaf area index, $r_{lu}$ is minimum leaf cuticular resistance, $H$ is gas-specific Henry Law constant, and $f_o$ is a reactivity factor for oxidation.

the advanced very high resolution radiometer for each PFT. As described in *Bonan et al.* [2002], CLM considers 15 PFTs based on the 24 biomes and the geographical distribution defined by *Olson et al.* [1983]. As an example, we show the global distribution of LAI and the seasonal cycle in the broadleaf deciduous temperate forest PFT in Figure S1 in the supporting information. Similarly, the calculation of $R_{lu}$ in the original dry deposition scheme neglects LAI, and we thus correct $R_{lu}$ to scale it over the bulk canopy [*Gao and Wesely*, 1995]. These errors in dry deposition are due to the implementation in the CESM (and MOZART) models, and are not inherent to the dry deposition schemes themselves.

Figure 1 shows $O_3$ deposition velocity and surface $O_3$ during the summer for the simulation without vegetation dependence in the dry deposition scheme (Original Scheme) and the changes in a simulation with

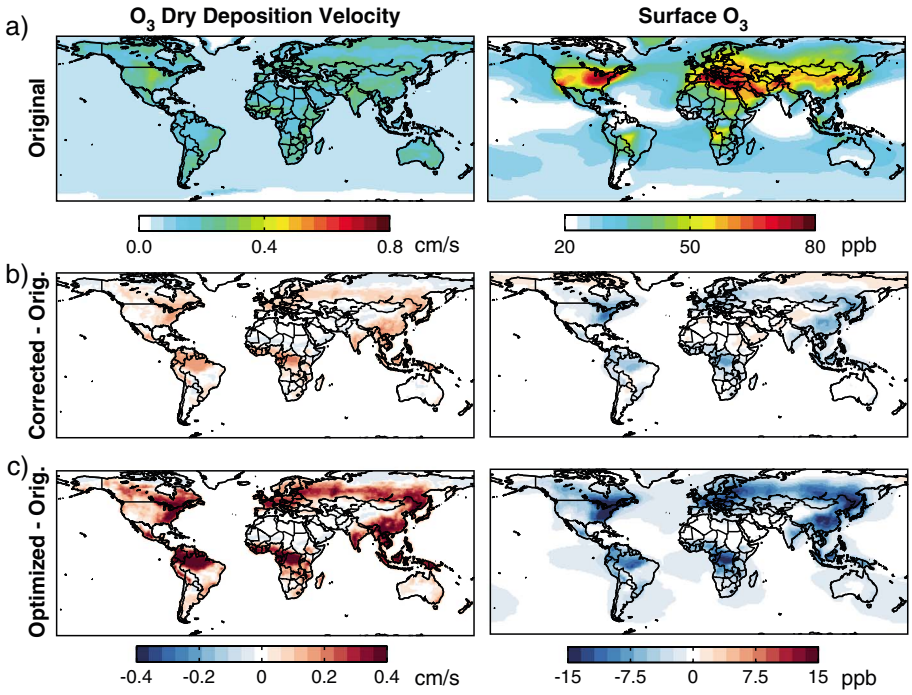


**Figure 1.** Dry deposition velocity (left) and surface $O_3$ (right) simulated by CESM during the summer (June, July, and August (JJA)) with the (a) "Original" dry deposition scheme. The difference between the LAI-coupled schemes and the original scheme are shown as (b) "Corrected Scheme"–"Original Scheme" and (c) "Optimized Scheme"–"Original Scheme".

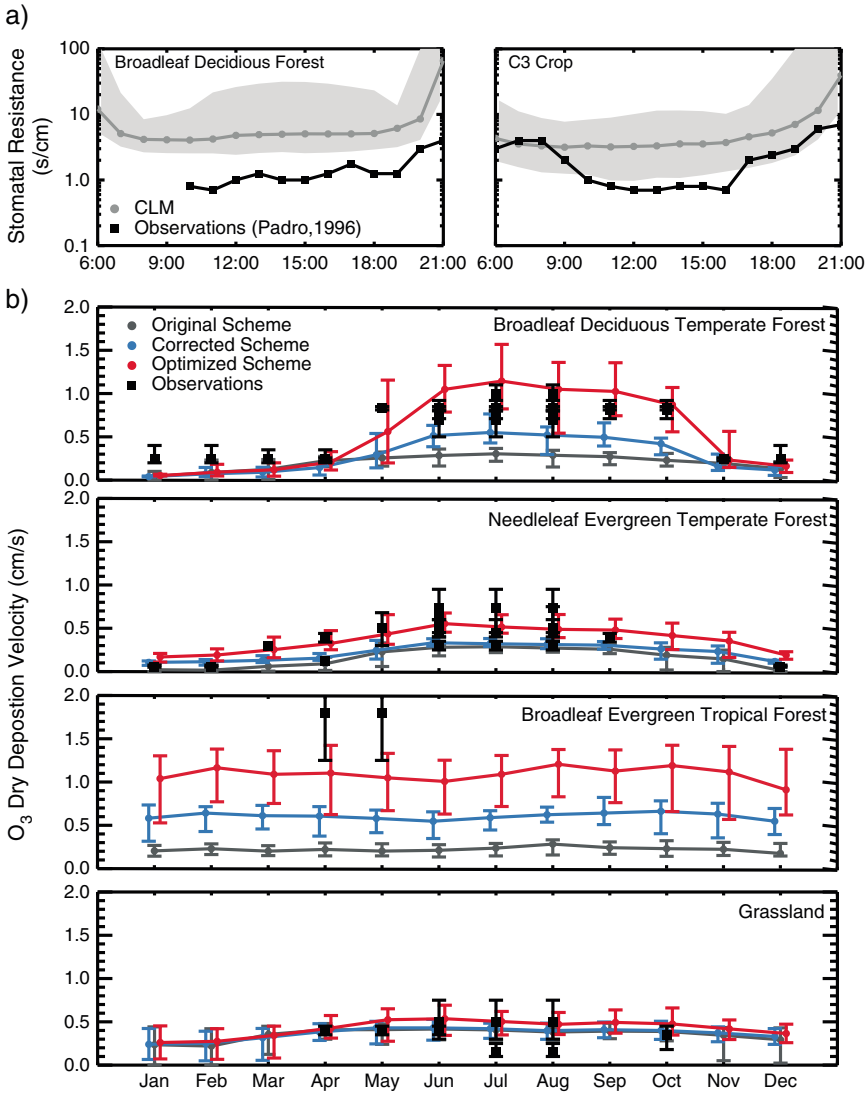


**Figure 2.** Comparison of modeled and observed (a) daytime stomatal resistance ($R_s$) and (b) midday $O_3$ dry deposition velocity ($V_d$). $R_s$ data show modeled median and minimum-maximum range (gray) and average from observations (black). $R_s$ observations are averages from measurements collected over a broadleaf deciduous forest in Ontario, Canada, and a cotton field in Sacramento, California, during the summer (JJA) [*Padro*, 1996]. $V_d$ observations (see Table 2) are shown in black, and results from three simulations are shown in grey (Original), blue (Corrected), and red (Optimized), respectively. Symbols show the mean values; vertical bars represent the minimum-maximum range.

vegetation dependence (Corrected Scheme). $O_3$ dry deposition and surface concentrations are substantially affected by linking the dry deposition scheme to LAI, in particular over densely vegetated regions. For example, the eastern U.S. is dominated by broadleaf deciduous forests and summertime LAI is about 4.5 (Figure S1). Deposition velocities increase by 0.25 cm/s (80% increase) with the Corrected Scheme. This leads to a decrease of 12 ppb of surface $O_3$ over the region in summertime.

To examine the performance of the original and corrected dry deposition schemes, we compare modeled $R_s$ with observations. We evaluate daytime $R_s$ because direct uptake through the stomata pores is the dominant $O_3$ removal process over vegetation; for most vegetation types, this uptake only occurs during the day as stomata are closed at night [e.g., *Wesely*, 1989; *Lamaud et al.*, 2002; *Wu et al.*, 2011]. Figure 2a displays daytime $R_s$ observations based on long-term measurements gathered in a broadleaf deciduous forest in Ontario, Canada, and a cotton field in Sacramento, California, during the summertime extracted from *Padro* [1996], Figure 2. We compare these observations to the simulated median $R_s$, and the minimum and maximum range from 6:00 to 21:00 local standard time (LST) during the summer for broadleaf deciduous

**Table 2.** A Review of Daytime $O_3$ Dry Deposition Velocities Over Main PFTs[a]

| Land Use Type | Location | High LAI[b] | Low LAI[b] |
|---|---|---|---|
| Deciduous Forest | Harvard Forest, MA | 0.81 (0.72–0.92) | |
| | Ontario, Canada | 1.0 (0.80–1.10) | 0.30 (0.20–0.35) |
| | Harvard Forest, MA | 0.70 (0.50–0.80) | 0.25 (0.20–0.40) |
| | Kane Experimental Forest, PA | 0.83 ± 0.015 | 0.24 ± 0.017 |
| Mixed Forest | Sand Flats State Forest, NY | 0.82 ± 0.013 | 0.55 ± 0.019 |
| | Duke Forest, NC | 0.80 (0.60–0.95) | |
| Coniferous Forest | Schefferville, Quebec | 0.30 (0.25–0.35) | |
| | Niwot Ridge Obs, CO | 0.55 (0.40–0.60) | |
| | Southern Norway | 0.45 (0.40–0.6) | 0.05 (0.05–0.075) |
| | Ulborg Forest, Denmark | 0.73 (0.45–0.95) | 0.39 (0.34–0.44) |
| | Les Landes Forest, France | 0.62 | 0.29 |
| | Niwot Ridge Obs, CO | 0.5 (0.3–0.68) | 0.12 |
| | Manitou Forest Obs, CO | 0.5 (0.35–0.75) | |
| Tropical Forest | Ducke, Amazon, Brazil | 1.8 (1.25–2.6) | |
| Cotton Field | Sacramento, CA | 0.75 (0.50–0.90) | |
| Grassland | Sacramento, CA | 0.15 (0.10–0.25) | |
| | Sand Mountains, AL | 0.4 (0.35–0.45) | |
| | Kansas, USA | 0.50 (0.30–0.75)[c] | 0.35 (0.18–0.45)[c] |

[a]Reported daytime (9:00–15:00 LST) $V_d$ as average (minimum-maximum), avg ± SD or average. Data extracted from *Wu et al.* [2011], *Padro et al.* [1991], *Padro et al.* [1992], *Munger et al.* [1996], *Finkelstein et al.* [2000], *Kumar et al.* [1983], *Hole et al.* [2004], *Mikkelsen et al.* [2000], *Lamaud et al.* [2002], *Turnipseed et al.* [2009], *Park et al.* [2014], *Fan et al.* [1990], *Padro et al.* [1994], *Meyers et al.* [1998], and *Gao and Wesely* [1995].

[b]High LAI are periods with active plant growth and large LAI and Low LAI are periods with no plant growth or/and snow cover (see text for further explanation).

[c]$V_d$ for 10:00–14:00.

temperate forests and C3 crops at those locations. The diurnal variability of $R_s$ is mainly regulated by radiation, which controls stomatal opening. During the day, $R_s$ decreases rapidly and reaches a minimum around local noon when stomata are fully open and vegetation photosynthesis activity is at a maximum [e.g., *Wesely*, 1989; *Padro*, 1996]. Observed daytime $R_s$ values range from 0.7 to 6 s/cm in both PFTs, and noon minima are 1 s/cm and 0.7 s/cm in the broadleaf deciduous temperate forest and cotton field, respectively. Similar daytime $R_s$ values have been reported in other, however limited, studies. *Finkelstein et al.* [2000] measured daytime average $R_s$ values of 2–6.4 s/cm over different broadleaf deciduous temperate trees; *Grantz et al.* [1997] reported daytime $O_3$ $R_s$ of 1.4–6.6 s/cm inferred from water vapor stomatal conductance measurements in a cotton field. The Ball-Berry $R_s$ scheme implemented in CESM captures the diurnal variability of observed $R_s$. However, the model substantially overestimates the $R_s$ magnitude by a factor of 5. *Lombardozzi et al.* [2012] suggest that $O_3$ damage to plants (not included here) would further increase the stomatal resistance; including this effect would exacerbate the model bias in stomatal resistance. Canopy parameters used to calculate $R_s$ are not well constrained in CLM4, and that may contribute to the large $R_s$ values [*Bonan et al.*, 2011]. It is also important to note that $R_s$ is difficult to measure, and observations are rather limited. Therefore, other sources of uncertainty may account for or contribute to the difference observed between the model and observations. However, it is unlikely that vegetation density is a major factor here. We find that a 50% increase in the LAI increases summertime midday $V_d$ by about 20%, with a concurrent decrease of 3 ppb in surface $O_3$ concentrations. Therefore, we use this initial model-observation comparison to optimize the $R_s$ values implemented in our dry deposition scheme.

Figure 1c shows results from a simulation in which we reduce the $R_s$ used in the dry deposition scheme by a factor of 5 to match the observations shown in Figure 2a (Optimized Scheme). This Optimized Scheme also includes the updated vegetation dependence of the Corrected Scheme. The impact of the Optimized Scheme on the ozone simulation is substantial. For example, in the eastern U.S. dry deposition velocities are 0.5 cm/s (~200%) larger than the Original Scheme, with a concurrent decrease of 20 ppb in surface $O_3$ concentrations. We observe similar decreases in surface $O_3$ over dense vegetated regions in the tropical Southern Hemisphere (e.g., Amazon) where LAI is large (~ 5) throughout the year.

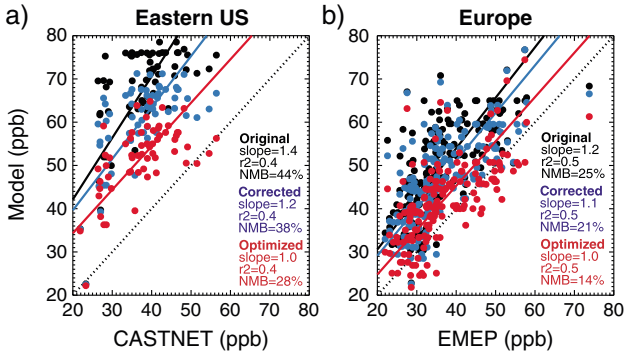


**Figure 3.** Scatterplots of simulated surface $O_3$ during the summer (JJA) with the Original Scheme (black), Corrected Scheme (blue) and Optimized Scheme (red) versus observed long-term mean values at (a) individual Clean Air Status and Trends Network (CASTNET) sites (1995–2005) in eastern U.S. and (b) individual European Monitoring and Evaluation Programme (EMEP) sites (1990–2009) in Europe. Squared-correlation coefficients ($r^2$), slope, and normalized mean biases (NMB) are shown in the inset. Reduced–major axis regression lines (solid) and the 1:1 lines (dash) are also shown.

To further support the changes suggested by our Corrected and Optimized schemes, we compare simulated ozone dry deposition velocities with observations in Figure 2b. We show the seasonal variation of $O_3$ $V_d$ over four sites (Harvard Forest (MA, USA), Rocky Mountain National Park (CO, USA), the Amazon (Brazil), and Kansas (USA)) representative of four major PFTs (broadleaf deciduous temperate forest, needleleaf evergreen temperate forest, broadleaf evergreen tropical forest, and grassland). We show the monthly average of midday (9:00–15:00 LST) $V_d$ as well as the minimum and the maximum values simulated by CESM at these locations. Table 2 summarizes midday $V_d$ from field observations reported in the literature over different PFTs. We report midday $V_d$ for high LAI and low LAI periods to distinguish the effect of growth and vegetation density on the deposition velocity. We define "high LAI" as periods with active plant growth and large LAI and "low LAI" as periods with no plant growth or/and snow cover, as defined in each study. Figure 2b includes observations from four of these PFTs, shown as the average and minimum and maximum (or ± standard deviation (SD)) reported in each study for the duration of measurement period. The comparison of $O_3$ $V_d$ observations from a particular location with global CESM model output (1.9° ×2.5° horizontal resolution) may be biased because of heterogeneity within the grid box. However, we ensure that the grid box, from which the model data are extracted, is dominated by the PFT in which observations were collected. Figure 2b shows that the ozone dry deposition is generally underestimated (in some cases by more than a factor of two) in the Original Scheme and both our Corrected and Optimized schemes improve comparisons with observations. The dry deposition velocity is particularly sensitive to $R_s$ under densely vegetated (high LAI) conditions. For example, the Optimized Scheme produces $V_d$ values that are a factor of two larger than the Corrected Scheme in deciduous forests during the summer and tropical forests throughout the year (~1 cm/s versus 0.5 cm/s), whereas it remains nearly constant in all configurations in deciduous forests during the winter (~0.1 cm/s) and grasslands (~0.3 cm/s).

In broadleaf deciduous temperate forests, $V_d$ is primarily controlled by the seasonal cycle of LAI (Figure S1) [e.g., *Finkelstein et al.*, 2000; *Wu et al.*, 2011]. Observations show a pronounced seasonality in $V_d$ with larger values from late spring to early fall (~0.8 cm/s in summer versus 0.1 cm/s in winter; Table 2). It is clear that the original dry deposition scheme configuration has little skill in capturing the seasonal variability of $V_d$. The new schemes dependent on LAI reproduce the seasonal cycle, with the Optimized Scheme capturing both the variability and the magnitude of the cycle. Similar results are found in needleleaf evergreen temperate forests, with a much less pronounced seasonality in the simulated and observed $V_d$.

In broadleaf evergreen tropical forests and grasslands, modeled and observed $V_d$ show little to no seasonality. In these PFTs, where LAI remains nearly constant throughout the year [e.g., *Turnipseed et al.*, 2009; *Gao and Wesely*, 1995], $V_d$ is mainly driven by environmental factors, such as temperature, humidity, light, and the presence of snow. In broadleaf evergreen tropical forests, the Optimized Scheme improves the comparison with observed dry deposition velocities but is still biased low. It is important to note that $V_d$ observations over tropical regions are very scarce, and data shown are based on only one field campaign (Table 2). In grasslands, dry deposition is not very sensitive to vegetation as LAI is very low (<1; Figure S1), and all configurations reproduce the observed ozone dry deposition velocities.

Figure 3 shows how these changes to the simulation of dry deposition affect the comparison of simulated surface $O_3$ concentrations with observations during the summer. In this comparison, we focus on the eastern United States and Europe since these are regions with dense observational networks and where a consistent positive bias in simulated surface $O_3$ has previously been identified. Observations shown for the eastern U.S. and Europe are long-term means from the CASTNET and EMEP networks, respectively. As an example, we show the bias between model and observations with the original dry deposition scheme in Figure S2 (supporting information). Over the eastern U.S. (Figure 3a), the simulation of surface $O_3$ concentrations is positively biased with all dry deposition scheme configurations. However, including LAI in the dry deposition scheme significantly improves the simulation of surface $O_3$. The Original Scheme has a mean positive bias of 30 ppb with respect to the observations, i.e., a 44% normalized mean bias (NMB), which is similar to that obtained for other periods studied with CESM [*Lamarque et al.*, 2012], and is clearly outside of the range of climate variability in surface $O_3$. This bias drops to 23 ppb (38% NMB) in the Corrected Scheme and to 14 ppb (28% NMB) in the Optimized Scheme. Over Europe (Figure 3b), all model configurations also tend to overestimate surface $O_3$. However, both the Corrected Scheme and Optimized Scheme are substantially closer to observations (respectively, 5 and 10 ppb bias versus 13 ppb in the Original Scheme). A more detailed evaluation using ozone sondes and satellite and aircraft observations shows that the updates to the dry deposition scheme have a negligible effect on $O_3$ concentrations above 900 hPa, and away from regions and periods with dense vegetation, i.e., eastern U.S. and Europe during the summer and Southern Hemisphere tropical regions (S. Tilmes, National Center for Atmospheric Research (NCAR), personal communication, 2014). Therefore, while the simulation of surface ozone is dramatically impacted by the representation of vegetation phenology in the dry deposition scheme, the global tropospheric ozone budget is largely unaffected. In addition, our changes to the dry deposition scheme have little impact on the simulation of other species (e.g., $SO_4$, $NO_2$, and CO), which are less sensitive to dry deposition losses [e.g., *Wesely*, 1989].

## 3. Conclusions

Dry deposition represents an important physical mechanism controlling surface $O_3$ in CESM. Correcting the vegetation dependence and optimizing the stomatal resistance used in the dry deposition scheme in CESM leads to a substantial improvement in the simulation of surface $O_3$ over regions that are well known to have a positive bias (e.g., eastern U.S. and Europe). Thus, ozone biases reported in the literature [e.g., *Murazaki and Hess*, 2006; *Lamarque et al.*, 2012] using the Original Scheme can, at least in part, be attributed to important oversimplifications in the implementation of the dry deposition scheme. Ensuring that models correctly link ozone deposition processes with vegetation and use accurate dry deposition schemes may be a first step toward improving surface $O_3$ simulations. However, our Optimized Scheme is based on limited observational constraints, and additional globally distributed measurements of both stomatal resistance and dry deposition velocities could be used to improve this parameterization. Further work is also needed to fully understand the causes of the bias in the simulated stomatal resistance, and the impact that the scaling applied in our Optimized Scheme may have on the simulation of the hydrological and carbon cycle, via greater stomatal water loss and carbon uptake. Finally, including explicit links between vegetation parameters and dry deposition is critical to the ability of Earth System Models to simulate surface $O_3$ response to future and past vegetation changes, as well as factors controlling changes in stomatal resistance, such as changes in $CO_2$ and drought stress. Thus, on-going investigation of the accuracy of such links must proceed concurrently with efforts to project changing global air quality.

**Acknowledgments**

This work was supported by the U.S. National Park Service (grant H2370 094000/J2350103006), the U.S. National Science Foundation (AGS-1238109), and the JFSP (project ID 13-1-01-4). We thank Sam Levis (NCAR), Gordon Bonan (NCAR), Louisa Emmons (NCAR), J-F Lamarque (NCAR), and Bill Munger (Harvard) for helpful discussions and Simone Tilmes (NCAR) for running a full diagnostic on the CESM output. S.R.A. acknowledges support from the NCAR Advanced Study Program and NCAR Atmospheric Chemistry Division. The CESM project is supported by the National Science Foundation and the Office of Science (BER) of the US Department of Energy. Computing resources were provided by the Climate Simulation Laboratory at NCAR's Computational and Information Systems Laboratory (CISL), sponsored by the National Science Foundation and other agencies. Any opinions, findings, and conclusions or recommendations expressed in this material are those of the author(s) and do not necessarily reflect the views of the National Science Foundation.

The Editor thanks two anonymous reviewers for their assistance in evaluating this paper.

## References

Baldocchi, D. D., B. B. Hicks, and P. Camara (1987), A canopy stomatal resistance model for gaseous deposition to vegetated surfaces, *Atmos. Environ.*, *21*(1), 91–101, doi:10.1016/0004-6981(87)90274-5.

Bonan, G. B., S. Levis, L. Kergoat, and K. W. Oleson (2002), Landscapes as patches of plant functional types: An integrating concept for climate and ecosystem models, *Global Biogeochem. Cycles*, *16*(2), 1021, doi:10.1029/2000GB001360.

Bonan, G. B., P. J. Lawrence, K. W. Oleson, S. Levis, M. Jung, M. Reichstein, D. M. Lawrence, and S. C. Swenson (2011), Improving canopy processes in the Community Land Model version 4 (CLM4) using global flux fields empirically inferred from FLUXNET data, *J. Geophys. Res.*, *116*, G02014, doi:10.1029/2010JG001593.

Collatz, G., J. Ball, C. Grivet, and J. A. Berry (1991), Physiological and environmental regulation of stomatal conductance, photosynthesis and transpiration: A model that includes a laminar boundary layer, *Agric. For. Meteorol.*, *54*(24), 107–136, doi:10.1016/0168-1923(91)90002-8.

Emmons, L. K., et al. (2010), Description and evaluation of the Model for Ozone and Related chemical Tracers, version 4 (MOZART-4), *Geosci. Model Dev.*, *3*(1), 43–67, doi:10.5194/gmd-3-43-2010.

Fan, S.-M., S. C. Wofsy, P. S. Bakwin, D. J. Jacob, and D. R. Fitzjarrald (1990), Atmosphere-biosphere exchange of $CO_2$ and $O_3$ in the central Amazon Forest, *J. Geophys. Res.*, *95*(D10), 16,851–16,864, doi:10.1029/JD095iD10p16851.

Finkelstein, P. L., T. G. Ellestad, J. F. Clarke, T. P. Meyers, D. B. Schwede, E. O. Hebert, and J. A. Neal (2000), Ozone and sulfur dioxide dry deposition to forests: Observations and model evaluation, *J. Geophys. Res.*, *105*(D12), 15,365–15,377, doi:10.1029/2000JD900185.

Fiore, A. M., et al. (2009), Multimodel estimates of intercontinental source-receptor relationships for ozone pollution, *J. Geophys. Res.*, *114*, D04301, doi:10.1029/2008JD010816.

Ganzeveld, L., L. Bouwman, E. Stehfest, D. P. van Vuuren, B. Eickhout, and J. Lelieveld (2010), Impact of future land use and land cover changes on atmospheric chemistry-climate interactions, *J. Geophys. Res.*, *115*, D23301, doi:10.1029/2010JD014041.

Gao, W., and M. Wesely (1995), Modeling gaseous dry deposition over regional scales with satellite observations: Model development, *Atmos. Environ.*, *29*(6), 727–737, doi:10.1016/1352-2310(94)00284-R.

Grantz, D., X. Zhang, W. Massman, A. Delany, and J. Pederson (1997), Ozone deposition to a cotton (Gossypium hirsutum l.) field: Stomatal and surface wetness effects during the California Ozone Deposition Experiment, *Agric. For. Meteorol.*, *85*(12), 19–31, doi:10.1016/S0168-1923(96)02396-9.

Hole, L., A. Semb, and K. Tayseth (2004), Ozone deposition to a temperate coniferous forest in Norway; Gradient method measurements and comparison with the EMEP deposition module, *Atmos. Environ.*, *38*(15), 2217–2223, doi:10.1016/j.atmosenv.2003.11.042.

Kumar, A., F. Chen, D. Niyogi, J. Alfieri, K. Manning, M. Ek, and K. Mitchell (1983), Using photosynthesis-based canopy resistance model and new MODIS-based data to improve the presentation of vegetation transpiration in the Noah land surface model, *Tech. Rep. J3.1*. 22nd conference of hydrology, Am. Meteorol. Soc., New Orleans, La.

Lamarque, J.-F., et al. (2012), CAM-Chem: Description and evaluation of interactive atmospheric chemistry in the Community Earth System Model, *Geosci. Model Dev.*, *5*(2), 369–411, doi:10.5194/gmd-5-369-2012.

Lamaud, E., A. Carrara, Y. Brunet, A. Lopez, and A. Druilhet (2002), Ozone fluxes above and within a pine forest canopy in dry and wet conditions, *Atmos. Environ.*, *36*(1), 77–88, doi:10.1016/S1352-2310(01)00468-X.

Lapina, K., D. K. Henze, J. B. Milford, M. Huang, M. Lin, A. M. Fiore, G. Carmichael, G. G. Pfister, and K. Bowman (2014), Assessment of source contributions to seasonal vegetative exposure to ozone in the US, *J. Geophys. Res. Atmos.*, *119*, 324–340, doi:10.1002/2013JD020905.

Lombardozzi, D., J. Sparks, G. Bonan, and S. Levis (2012), Ozone exposure causes a decoupling of conductance and photosynthesis: Implications for the Ball-Berry stomatal conductance model, *Oecologia*, *169*(3), 651–659, doi:10.1007/s00442-011-2242-3.

Meyers, T. P., P. Finkelstein, J. Clarke, T. G. Ellestad, and P. F. Sims (1998), A multilayer model for inferring dry deposition using standard meteorological measurements, *J. Geophys. Res.*, *103*(D17), 22,645–22,661, doi:10.1029/98JD01564.

Mikkelsen, T., H. Ro-Poulsen, K. Pilegaard, M. Hovmand, N. Jensen, C. Christensen, and P. Hummelshoej (2000), Ozone uptake by an evergreen forest canopy: Temporal variation and possible mechanisms, *Environ. Pollut.*, *109*(3), 423–429, doi:10.1016/S0269-7491(00)00045-2.

Munger, J. W., S. C. Wofsy, P. S. Bakwin, S.-M. Fan, M. L. Goulden, B. C. Daube, A. H. Goldstein, K. E. Moore, and D. R. Fitzjarrald (1996), Atmospheric deposition of reactive nitrogen oxides and ozone in a temperate deciduous forest and a subarctic woodland: 1. Measurements and mechanisms, *J. Geophys. Res.*, *101*(D7), 12,639–12,657, doi:10.1029/96JD00230.

Murazaki, K., and P. Hess (2006), How does climate change contribute to surface ozone change over the United States?, *J. Geophys. Res.*, *111*, D05301, doi:10.1029/2005JD005873.

Neale, R. B., J. Richter, S. Park, P. H. Lauritzen, S. J. Vavrus, P. J. Rasch, and M. Zhang (2013), The mean climate of the community atmosphere model (CAM4) in forced SST and fully coupled experiments, *J. Clim.*, *26*, 5150–5168, doi:10.1175/JCLI-D-12-00236.

Oleson, K. W., et al. (2010), Technical description of version 4.0 of the Community Land Model (CLM), *Tech. Rep. Technical Note NCAR/TN-478+STR,* 257 pp. NCAR.

Olson, J. S., J. A. Watts, and L. J. Allison (1983), Carbon in live vegetation of major world ecosystems, *Tech. Rep. ORNL-5862*. Oak Ridge Natl. Lab., Oak Ridge, Tenn.

Padro, J. (1996), Summary of ozone dry deposition velocity measurements and model estimates over vineyard, cotton, grass and deciduous forest in summer, *Atmos. Environ.*, *30*(13), 2363–2369, doi:10.1016/1352-2310(95)00352-5.

Padro, J., G. den Hartog, and H. Neumann (1991), An investigation of the ADOM dry deposition module using summertime $O_3$ measurements above a deciduous forest, *Atmos. Environ.*, *25*(8), 1689–1704, doi:10.1016/0960-1686(91)90027-5.

Padro, J., H. Neumann, and G. Hartog (1992), A wintertime comparison of modelled and observed dry deposition velocity of $O_3$ over a deciduous forest, in *Air Pollution Modeling and Its Application IX, NATO Challenges of Modern Society*, vol. 17, edited by H. Dop and G. Kallos, pp. 495–501, Springer, New York, doi:10.1007/978-1-4615-3052-749.

Padro, J., W. Massman, R. Shaw, A. Delany, and S. Oncley (1994), A comparison of some aerodynamic resistance methods using measurements over cotton and grass from the 1991 California ozone deposition experiment, *Boundary Layer Meteorol.*, *71*(4), 327–339, doi:10.1007/BF00712174.

Park, R. J., S. K. Hong, H.-A. Kwon, S. Kim, A. Guenther, J.-H. Woo, and C. P. Loughner (2014), An evaluation of $O_3$ dry deposition simulations in East Asia, *Atmos. Chem. Phys. Discuss.*, *14*(1), 919–951, doi:10.5194/acpd-14-919-2014.

Reidmiller, D. R., et al. (2009), The influence of foreign vs. North American emissions on surface ozone in the US, *Atmos. Chem. Phys.*, *9*(14), 5027–5042, doi:10.5194/acp-9-5027-2009.

Sanderson, M. G., C. D. Jones, W. J. Collins, C. E. Johnson, and R. G. Derwent (2003), Effect of climate change on isoprene emissions and surface ozone levels, *Geophys. Res. Lett.*, *30*(18), 1936, doi:10.1029/2003GL017642.

Sanderson, M. G., W. J. Collins, D. L. Hemming, and R. A. Betts (2007), Stomatal conductance changes due to increasing carbon dioxide levels: Projected impact on surface ozone levels, *Tellus B*, *59*(3), 404–411, doi:10.1111/j.1600-0889.2007.00277.x.

Sellers, P. J., S. O. Los, C. J. Tucker, C. O. Justice, D. A. Dazlich, G. J. Collatz, and D. A. Randall (1996), A revised land surface parameterization (SiB2) for atmospheric GCMS. Part II: The generation of global fields of terrestrial biophysical parameters from satellite data, *J. Clim.*, *9*, 706–737, doi:10.1175/1520-0442(1996)009<0706:ARLSPF>2.0.CO;2.

Turnipseed, A. A., S. P. Burns, D. J. Moore, J. Hu, A. B. Guenther, and R. K. Monson (2009), Controls over ozone deposition to a high elevation subalpine forest, *Agric. For. Meteorol.*, *149*(9), 1447–1459, doi:10.1016/j.agrformet.2009.04.001.

Wesely, M. (1989), Parameterization of surface resistances to gaseous dry deposition in regional-scale numerical models, *Atmos. Environ.*, *23*(6), 1293–1304, doi:10.1016/0004-6981(89)90153-4.

Wild, O. (2007), Modelling the global tropospheric ozone budget: Exploring the variability in current models, *Atmos. Chem. Phys.*, *7*(10), 2643–2660, doi:10.5194/acp-7-2643-2007.

Wu, S., L. J. Mickley, D. J. Jacob, J. A. Logan, R. M. Yantosca, and D. Rind (2007), Why are there large differences between models in global budgets of tropospheric ozone?, *J. Geophys. Res.*, *112*, D05302, doi:10.1029/2006JD007801.

Wu, S., L. J. Mickley, J. O. Kaplan, and D. J. Jacob (2012), Impacts of changes in land use and land cover on atmospheric chemistry and air quality over the 21st century, *Atmos. Chem. Phys.*, *12*(3), 1597–1609, doi:10.5194/acp-12-1597-2012.

Wu, Z., et al. (2011), Evaluating the calculated dry deposition velocities of reactive nitrogen oxides and ozone from two community models over a temperate deciduous forest, *Atmos. Environ.*, *45*(16), 2663–2674, doi:10.1016/j.atmosenv.2011.02.063.

Zhang, L., J. R. Brook, and R. Vet (2002), On ozone dry deposition with emphasis on non-stomatal uptake and wet canopies, *Atmos. Environ.*, *36*(30), 4787–4799, doi:10.1016/S1352-2310(02)00567-8.